In Situ Infrared Measurements on TiO_2 Flames: Gas and Particle Concentrations

Osama I. Arabi-Katbi and Sotiris E. Pratsinis
Dept. of Chemical Engineering, University of Cincinnati, Cincinnati, OH 45221

Philip W. Morrison, Jr.
Dept. of Chemical Engineering, Case Western Reserve University, Cleveland, OH 44106

Fourier transform infrared spectroscopy was performed on premixed flames of titanium tetraisopropoxide, methane and oxygen. A combination of emission/transmission (E/T) measurements yields gas temperature, gas concentrations, soot temperature, soot concentration and absorption features of TiO_2 particles. To validate the temperature measurements, a thermocouple is inserted into the IR path within the flame, and its temperature is compared to the surface temperature from E/T analysis which agrees quite well. The HITEMP and HITRAN databases are used to determine the gas mol fractions in the flame. Soot is observed in the emission spectra of the flame, and its concentration decreases with its increasing position above the burner. The soot temperature is always less than the gas temperature. The IR feature of TiO_2 particles is hard to observe, because it is very small relative to H_2O and CO_2 features. Interfering features, however, were removed using either calculated spectra or by experimentally generating a reference flame using an acetone–methane flame.

Introduction

Temperature measurements employing conventional thermocouple probing in nonsooting flames can give relatively accurate results, but when soot or particles are formed in the flame, such measurements become less accurate (Kent and Wagner, 1984). Madson and Theby (1984) studied the use of thermocouples to measure temperatures in nonequilibrium, high-temperature reactive gas flows by comparing the measured gas temperature in a SiO_2 flame with particle-coated and noncoated thermocouples. They found that a significant error occurs in flame temperature measurements due to catalytic heating when platinum and or other transition metal wire is used in the thermocouple.

In addition to conventional thermocouple insertion, various other methods have been used to measure flame temperatures. Kent and Wagner (1984) first successfully used a rapid-insertion technique, which allows for the insertion of a thermocouple into a flame for a well-defined time using a rapid-insertion instrument. Govatzidakis (1993) also used this technique to obtain axial and radial temperatures in laminar diffusion flames. Boedeker and Dobbs (1986) and Farrow et al. (1984) used coherent anti-Stokes Raman spectroscopy (CARS), while Bengtsoon et al. (1992) used rotational CARS thermometry to obtain flame temperature.

Fourier transform infrared (FTIR) spectroscopy has also been used in various applications for measuring hot gas temperature and was found to be in good agreement with other temperature measurement techniques (Solomon et al., 1986). Best et al. (1986) showed that the use of combined spectral emission/transmission (E/T) infrared provided information on hot gas temperature in an ethylene diffusion flame. The transmission measurements yield information on the gas-phase composition, particle composition, mass fraction, and size; emission measurements contain information on the temperature of the gases and particles (Best et al., 1986). They found that the particle temperature measurements made by this technique can be as accurate as ± 25 K. Solomon et al. (1986) also used FTIR E/T as an *in situ* combustion diagnostic of an ethylene diffusion flame, and found that the FTIR

Correspondence concerning this article should be addressed to P. W. Morrison, Jr.
Present address of S. E. Pratsinis: Institute of Process Engineering, ETH Zurich, CH-8092 Zurich, Switzerland.
Present address of O. I. Arabi-Katbi: Degussa Corporation, 4301 Degussa Rd., Theodore, AL 36590.

temperature measurements are accurate to within ± 50 K when compared with other methods, such as thermocouples or CARS (Best et al., 1991). In addition, Best et al. (1991) used the FTIR to observe soot, as well as other forms of hydrocarbon complexes in the ethylene diffusion flame. When coupled with tomographic reconstruction, these authors found that the soot temperature differs from the gas temperature at the same location over large regions of the flame, with a maximum difference of 360 K. In a similar work, Markham et al. (1990) studied the combustion of a coal flame using FTIR and determined point values for species temperatures and relative concentrations. They used a Pt + Pt/Rh thermocouple at various positions in the flame. The thermocouple temperature was corrected for radiation losses using a 0.9 emissivity factor because of the soot and particles coating the surface. They also obtained values for particle temperature, relative particle density, relative soot concentration, relative radiance intensity, as well as relative CO_2 concentration and temperature as a function of distance from the flame axis and height above the coal injection nozzle. They found that the highest CO_2 temperature ranged between 2,200 and 2,600 K, while the highest particle temperature ranged between 1,900 and 2,000 K. In other work, Morrison et al. (1990) studied diamond growth in an oxygen–acetylene flame using FTIR E/T analysis. They estimated temperatures for the various species in the flame and found that the temperature of CO_2 ranged between 2,800 and 3,300 with a variation of ± 50 K. Morrison et al. (1997) also used FTIR spectroscopy to study the effect of electrical fields on the flame synthesis of TiO_2 from the oxidation of $TiCl_4$. They observed that electrical fields increased flame temperature. The TiO_2 particle and the gas temperatures were found to be the same.

The primary objective of this work is to use E/T FTIR to map out the axial concentration profiles of gas and particle (TiO_2 and soot) concentrations for CH_4 flames containing the precursor, titanium tetraisopropoxide (TTIP). We have used these IR measurements to develop quantitative methods of measuring concentrations of gas species and particles as well as gain understanding of the competing roles of precursor pyrolysis and combustion in these flames. In contrast to our previous work (Morrison et al., 1997), a TTIP–CH_4 flame is used to synthesize TiO_2 particles so as to avoid the chloride chemistry of a $TiCl_4$–CH_4 flame. In addition, this work is an extension of our other results reported in Arabi-Katbi et al. (2000). In that work, we also applied *in situ* FTIR spectroscopy (as well as thermophoretic sampling) to study the role of the axial temperature profile in the formation and growth of TiO_2 particles in the TTIP–CH_4 flame. FTIR provided temperature information while thermophoretic sample was used to measure particle size. We found that the average primary particle size increases while the flame temperature decreases with increasing height in the flame. In contrast, this work measures the axial concentrations of gas species within the flame as a function of the TTIP flow rate. Calculation of reference spectra for the gases is possible using the HITRAN/HITEMP databases and the method of Morrison and Taweechokesupsin (1998). Another objective is to use FTIR measurements to determine the axial profile of the soot concentration in the TTIP–CH_4 flame as well as its temperature profile; soot is not found in the $TiCl_4$–CH_4 flames of Morrison et al. (1997). This information will improve our understanding of the role of precursor pyrolysis in the flame chemistry. A third objective is to show that by carefully removing hot H_2O and CO_2 absorption features from the flame spectra, we can detect the IR spectrum of the TiO_2 particles within the flame. Finally, we have reverified the accuracy of the E/T methodology by recording the E/T FTIR spectra from a thermocouple inserted in the CH_4 flame; after calculating the surface temperature of the thermocouple using the E/T measurements, we compare the surface temperature directly to the thermocouple's readout. A nonsooting methane flame is selected to avoid inaccuracies in the thermocouple readout due to particle deposition.

Experimental Procedures

Apparatus

The burner setup (Vemury and Pratsinis, 1996) appears in Arabi-Katbi et al. (2000). Methane (Praxair, 99.5%) is used as fuel, while oxygen (Praxair, 99.6%) is used as oxidant. Liquid titanium tetraisopropoxide (TTIP), $Ti(O—C_3H_7)_4$ (Aldrich, 97%) is heated to 125°C using heating tape. Burning TTIP [in contrast to $TiCl_4$ (Morrison et al., 1997)] provides less corrosive and relatively safer reactants and products. Using TTIP can also produce highly pure TiO_2 particles that are necessary for certain applications; the absence of HCl from the effluent stream of the process generates particles of much greater purity. Argon (Praxair, 99.99%) is first bubbled through a gas washing bottle [(bubbler), Corning] containing Drierite anhydrous $CaSO_4$ (size 8 mesh) to dry the gas, then passed through the bubbler containing the liquid TTIP to carry the TTIP vapor into the burner. Nitrogen (Praxair, 99.5%) is used as a diluting gas, as well as a sheath gas in the outside line in the burner. The sheath N_2 (6,000 cm^3/min) is fed through the outer ring of the burner to reduce the flame flicker and contact with the surrounding air. The gas flow rates are: 400–1,000 cm^3/min for Ar, 3,300–3,800 cm^3/min for diluting N_2, 1,200 cm^3/min for O_2, and 400 cm^3/min for CH_4. Different Ar and diluting N_2 flow rates are used to obtain different TTIP mass flow rates (Table 1). Downstream of the bubbler, all the gas lines are wrapped with heating tape to prevent any condensation of the precursor. A check valve is used to prevent any flame flashback. The burner (stainless steel, 2 cm ID) is packed to three-quarters of its volume with 5-mm glass beads supported on a screen. The flame is stabilized on the burner mouth using a 3.5-cm-long mullite monolith (Corning) honeycomb with 400 openings/in^2 (Vemury and Pratsinis, 1996). A burner-stabilized, premixed, flat flame is used here, as most of the particles experience

Table 1. Experimental Conditions and Flame Characteristics for Different TTIP Mass Flow Rates

Mass Flow Rate (g/h)	Argon Flow Rate (cm^3/min)	Diluting N_2 Flow Rate (cm^3/min)	Luminous Flame Height (cm)	Adiabatic Flame Temp. (K)	Fuel Equiv. Ratio (ϕ)*
4 (TTIP)	300	3,750	6.0	2,130	1.34
11 (TTIP)	400	3,850	7.0	2,355	1.13
15 (TTIP)	850	3,500	7.5	2,435	1.04

*ϕ is defined as the fuel/oxidizer ratio divided by the stoichiometric fuel/oxidizer ratio.

similar temperature and gas velocities across the flame (Vijayakumar and Whitby, 1984).

For the acetone [$CO(CH_3)_2$] flame experiments, acetone is placed in the gas washing bottle (bubbler) instead of the TTIP. The argon and diluting N_2 flow rates of the gases are included in Table 1, while the O_2, CH_4, and the outside N_2 remained the same as in the case of TTIP. No heating is applied to either the bubbler or the gas lines when acetone is used as a precursor because of its high vapor pressure.

Infrared measurements

The FTIR spectrometer used in this study is a Bomem MB157 operating over the spectral range 6,500–500 cm^{-1} with a resolution of 2 cm^{-1}. The spectrometer uses a wideband deuterated triglycine sulfate (DTGS) detector for the transmission measurements and a HgCdTe detector for the emission measurements. Two off-axis paraboloidal mirrors focus the IR through the flame, with a spot size of less than a 1 cm^2 (Morrison et al., 1997). The path correction spectrum for the emission measurements is taken using a blackbody cavity placed at the focus of the optics (Morrison and Haigis, 1993); a room temperature correction to the path correction is not required, since it will be small in comparison to the blackbody cavity and the flame emission. A background (transmission) spectrum is first taken with no flame and no source gases; the sheath N_2 stream is kept on. After the flame is ignited, a transmission spectrum is collected, followed by turning the IR source off in the spectrometer and collecting an emission spectrum. Twenty scans are taken for each of the transmission and emission spectra. For the measurements where the thermocouple is inserted in the flame, a (transmission) background spectrum is first taken without the thermocouple. Then the thermocouple is inserted in the path of the IR beam. The thermocouple was lowered into the focal spot from the top so as not to influence the gases upstream (see Results and Discussion for more details). The alignment option in the FTIR software (BGRAMS from Galactic, Inc.) is used to ensure that the area of the thermocouple tip actually blocks part of the IR beam. A 17% reduction of the IR signal is typical when the thermocouple is inserted in the IR path. Another (transmission) background is then taken before igniting the flame. A standard procedure is then followed by taking both transmission and emission spectra of the flame at the same location as the thermocouple. The thermocouple used is a K-type stainless steel (SS) thermocouple (Omega Engineering). The thermocouple temperature is corrected for heat loss according to Collis and Williams (1959). The emissivity factor for a carbon-coated thermocouple is 0.57 (Lide, 1982).

Emission/transmission analysis

The E/T analysis compares the normalized radiance calculated from the actual radiance of a sample to the best fit of a Planck function (Solomon and Best, 1991), where the Planck function spectra can be calculated according to Griffiths and de Haseth (1986). The normalized radiance, $R_n(\upsilon)$, of a sample can be calculated using:

$$R_n(\upsilon) = \frac{R(\upsilon)}{1-\tau(\upsilon)} \tag{1}$$

where $R(\upsilon)$ is the actual radiance and $\tau(\upsilon)$ is the transmittance of the flame. The normalized radiance is then compared to a Planck function at various temperatures $R_n(\upsilon) = BB\ (\upsilon, T)$, until a best match is achieved. The best match provides an average gas temperature of the sample flame.

HITRAN and HITEMP calculations

HITRAN and HITEMP databases are used to calculate the relative gas concentration (H_2O and CO_2) in the flame using the method of Morrison and Taweechokesupsin (1998). The method consists of using the spectroscopic parameters in HITRAN and HITEMP databases (Rothman et al., 1987, 1992) to calculate the gas spectrum at a given temperature, total pressure, and partial pressure. The HITRAN databases are used to obtain the desired spectrum at relatively low temperatures (less than 700 K), while the HITEMP databases are used to obtain the desired spectrum at the higher temperatures (1,400 to 2,200 K).

To briefly summarize this procedure (Morrison and Taweechokesupsin, 1998), we calculate a set of standard spectra at specific temperatures (700, 1,400, 1,600, 1,800, 2,000 or 2,200 K) and partial pressures (0.2 atm for H_2O or 0.1 atm for CO_2). All calculations use total pressure = 1 atm and a path length equal to 2 cm. The calculation accounts for all the major line-broadening mechanisms: Lorentzian (pressure broadening), Gaussian (temperature broadening), or Voigt (mixed broadening). The spectral ranges of interest for CO_2 are 900–500 cm^{-1} and 2,400–2,300 cm^{-1}, while for H_2O they are 1,000–500 cm^{-1} and 1,560–1,000 cm^{-1}. Once a high-resolution spectrum is calculated, an inverse Fourier transform is then applied to the spectrum to yield a synthetic interferogram. The interferogram is then apodized (triangle function) and truncated to the desired resolution (2 cm^{-1}) and Fourier transformed back to yield the 2 cm^{-1} resolution spectrum.

To calculate the mol fraction of H_2O and CO_2 using these standard spectra, we base-line correct the absorbance of the flame spectrum so the base line is very close to zero for comparison with the standard spectrum. The absorbance of the calculated HITEMP H_2O spectrum (calculated at the estimated average gas temperature from E/T analysis) is then obtained in the 1500–1100 cm^{-1} wavenumber range. This spectral range is selected because only water absorbs in this range. A least-square analysis is then used to obtain the relative magnitude of the experimental compared to the standard spectra:

$$\text{Relative magnitude} = \Sigma_\upsilon\left[(\text{ref}(\upsilon)\times\exp(\upsilon)\right]/\Sigma_\upsilon\left[\text{ref}(\upsilon)\right]^2,$$

where ref(υ) is the standard spectrum, exp(υ) is the experimental spectrum, and υ is the wavenumber (cm^{-1}). The relative magnitude is then multiplied by 20% (the mol fraction for the H_2O in the standard spectrum) to obtain the mol fraction of H_2O for the experimental spectrum.

Standard CO_2 bands were also simulated using HITRAN/HITEMP for different wavenumber ranges, but they were found not to be as accurate when compared to the experimental spectra due to the presence of H_2O in the same regions (1,000–500 cm^{-1}). Part of the difficulty may be due to an incomplete database of spectra lines found in HITRAN and HITEMP. As an alternative, one can infer the CO_2 con-

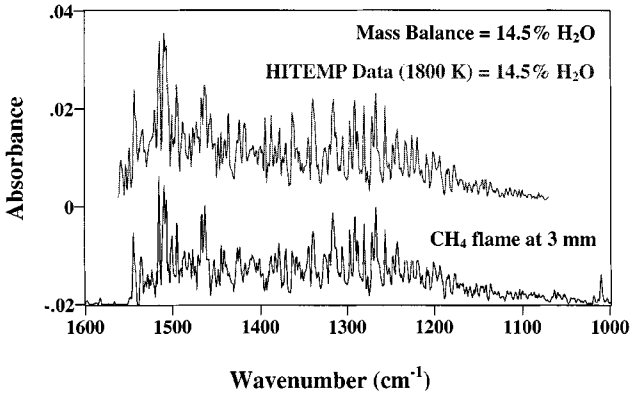

Figure 1. Measured H_2O spectrum in a CH_4 flame vs. H_2O spectrum calculated using the HITEMP database.

The two spectra are on the same scale, but the methane flame spectrum is offset by 0.02 absorbance units for clarity. The mol fraction 14.5% is calculated from an overall mass balance.

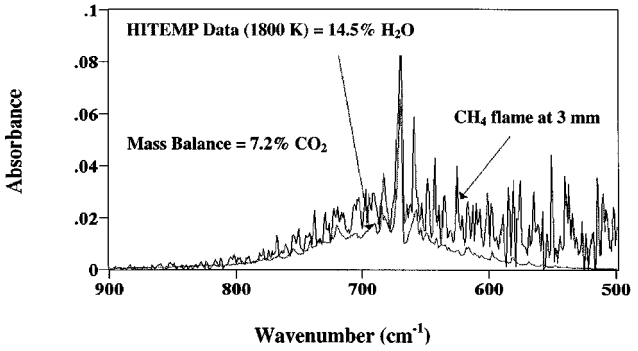

Figure 2. Measured CO_2 spectrum in a CH_4 flame vs. CO_2 spectrum calculated using the HITEMP database.

The mol fraction 7.2% is calculated from an overall mass balance.

centration using the measured H_2O mol fraction using the reaction stoichiometry. The CO_2 mol fraction is calculated, assuming all the TTIP and CH_4 in the flame have completely reacted to CO_2 and H_2O. For a TTIP-free flame, methane oxidation produces 2:1 mol ratio of H_2O:CO_2. For the case of a TTIP mass flow rate of 15 g/h (0.052 mol/h), the flow rates of the products are 2.88 mol/h H_2O (18%), 1.70 mol/h CO_2 (10.6%), and 11.4 mol/h argon and nitrogen (neglecting the small amounts of titania). Thus, the H_2O:CO_2 mol ratio is 1.7.

Results and Discussion

Species concentration at the burner mouth (closing the mass balance)

In a methane-only flame at $z = 3$ mm above the burner, the E/T temperature is measured as 1,800 K, and using the preceding method, the mol fraction of H_2O is measured as 14.4% (Figure 1). This result is in excellent agreement with the mol fraction calculated from the mass balance (14.5%), assuming the methane has been burned to H_2O and CO_2 (Figure 1). To verify the H_2O estimation, the absorbance of the HITEMP-simulated spectrum of H_2O (14.4% at 1,800 K in the 900–500-cm^{-1} wavenumber region) is shown in Figure 2.

Figure 2 shows the comparison of the measured CO_2 band (900–500 cm^{-1}) with a simulated spectrum calculated using HITEMP, temperature = 1,800 K, and a CO_2 mol fraction determined from the overall mass balance (7.2%). The predicted CO_2 concentration matches the *in situ* experimental CO_2 bands reasonably well (especially after removing the H_2O from the experimental spectrum), but nonetheless it is a slight underestimate. When we calculate the 2,350-cm^{-1} band of CO_2, the underestimate in the calculation is much more serious. The reason for this underestimate could be due to (1) missing spectral lines in the database, and/or (2) the strong absorption of the CO_2 bands makes CO_2 simulations more sensitive to using the average temperature (1,800 K) when calculating spectra because the true temperature profile is spatially averaged. Note that the CO_2 band in the 900–500-cm^{-1} region is significantly stronger than the H_2O spectrum in the 1,500–1,100-cm^{-1} region (scale change between Figure 1 and Figure 2); the 2,350-cm^{-1} band of CO_2 is even stronger (~ 0.15 absorbance units). Furthermore, the spot size of the FTIR beam is ~ 5 mm, which can cause significant spatial averaging in both the radial and axial direction (in addition to the line-of-sight averaging). Consequently, if the measurement of CO_2 using calculated spectra alone is not possible, calculating the CO_2 mol fraction from stoichiometry and the measured H_2O mol fraction of H_2O (in the region 1,500–1,100-cm^{-1}) is a reasonable alternative.

E/T analysis compared to thermocouple measurements

In these experiments, we compare the E/T measurements directly to thermocouple measurements. In a set of preliminary experiments, a thermocouple was placed directly inside the luminous methane flame (luminous height of 5 mm), but the flame climbed around the thermocouple, thus significantly perturbing the flame. To overcome this problem, the thermocouple is placed 10 mm above the burner (slightly above the luminous tip of the flame) so that there was little visual perturbation. The temperature reading of the thermocouple fluctuates slightly, but provides an average reading of around 800 ± 20°C.

When the thermocouple is inside the IR spot (Figure 3), the transmission area of the spot is reduced to $(1-f)\,A_o$, where f is the area of the IR beam blocked by the thermocouple, and A_o is the spot-size area. We can roughly estimate f by ratioing the centerburst of the interferogram with the thermocouple to the interferogram without the thermocouple ($f = 1 - I_{T/C}/I_{no\ T/C}$). When the thermocouple is partially blocking the IR focal spot, the portion of the radiance due to the thermocouple, $R_{T/C}(\upsilon)$, will be equal to

$$R_{T/C}(\upsilon) = f\epsilon(\upsilon)BB(\upsilon, T_{T/C}) \qquad (2)$$

where $\epsilon(\upsilon)$ is the emissivity of the thermocouple, and $BB(\upsilon, T_{T/C})$ is the Planck function at the temperature of the thermocouple $T_{T/C}$. The portion of radiance due to the gas,

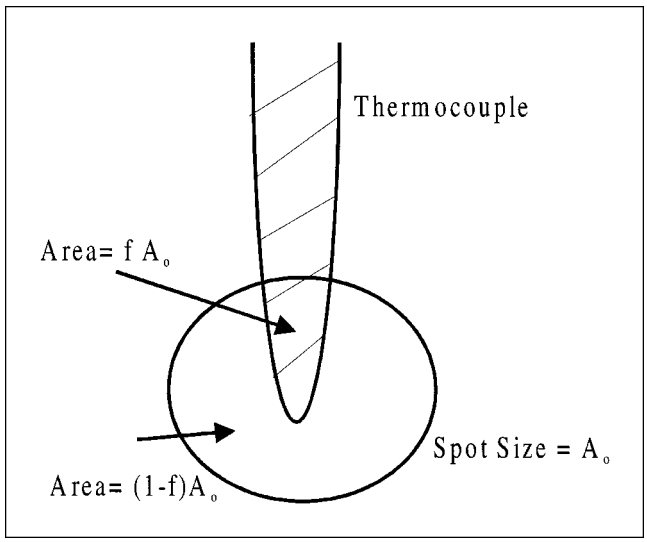

Figure 3. Thermocouple inserted in the IR path.

$R_{\text{gas}}(\upsilon)$, will be equal to

$$R_{\text{gas}}(\upsilon) = [1-\tau'(\upsilon)](1-f)BB(\upsilon, T_g), \qquad (3)$$

where $\tau'(\upsilon)$ is the transmission of the gas calculated using the background transmission taken with the thermocouple inserted in the spot, and T_g = gas temperature. In this analysis, we neglect the small contribution of the radiance of the gas in front of the thermocouple. The factor $(1-f)$ accounts for the fact that only a portion of the IR radiation from the hot gas reaches the detector. The total radiance (R) detected at the emission detector will be the sum of the radiance from both the thermocouple and the gas: $R = R_{T/C}(\upsilon) + R_{\text{gas}}(\upsilon)$.

Figure 4 shows the radiance (emission) of the TTIP-free methane flame with the thermocouple inserted inside the flame (10 mm above the tip of burner). The presence of the thermocouple raises the "base line" of the radiance spectrum above zero. To determine the thermocouple temperature from the radiance, we can assume that the emissivity $\epsilon(\upsilon)$ is independent of wavenumber, and thus fit a graybody to the base line of the radiance. Specifically, we fit the graybody to the radiance in the wavenumber ranges of 2,630–5,900 and 6,100–6,500 cm^{-1} by using $T_{T/C}$ and the quantity $f\epsilon$ as adjustable parameters. In Figure 4, the fit shows a temperature of 1,068 K (795°C), which is very comparable to the thermocouple temperature readout (800°C). When calculating this graybody temperature for the uncorrected radiance spectrum when the thermocouple is placed 5 mm above the burner (inserted in the flame), the best-fit graybody temperature is 1,158 K (885°C), an even more accurate prediction of the thermocouple temperature, 890°C.

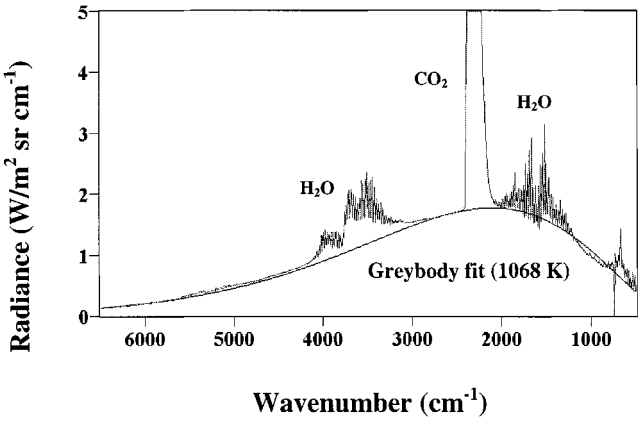

Figure 4. Best-fit graybody temperature for the thermocouple radiance spectrum.

The spectrum is taken in a premixed methane flame, with the thermocouple inside the flame and 10 mm above the burner.

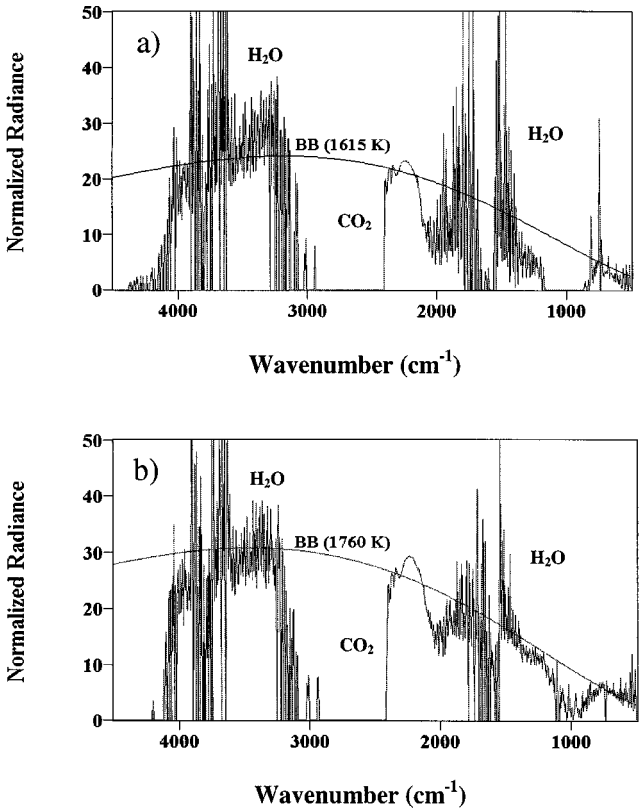

Figure 5. Normalized radiance spectra of the hot gases of a premixed methane flame using E/T analysis.

(a) With thermocouple (after base-line correction to remove thermocouple radiation); (b) without thermocouple.

Figure 5a shows the normalized radiance spectrum of the hot gases in the TTIP-free methane flame, with the thermocouple placed in the path of the IR beam. It is important to note here that the base line shift of the radiance spectrum is removed, using the graybody fit as a base line. A slightly higher E/T temperature (1,760 K compared to 1,615 K) is obtained for the same hot gases when the thermocouple is removed from the IR beam (Figure 5b). The reason for this is the fact that the thermocouple is a cold object, and it reduces the hot gas temperature measured by the IR beam.

The emissivity factor for a carbon-coated SS thermocouple is 0.57 (Lide, 1982). Note that the emissivity factor will be larger when soot and particles deposit on the thermocouple (Markham et al., 1990). Using 0.57 for an emissivity factor and the different experimental conditions to calculate the heat loss from the thermocouple, one can correct the measured thermocouple temperature of $T_{T/C} = 1{,}073$ K to estimate a gas temperature of 1,631 K. This value is very comparable to the temperature calculated by E/T analysis (1,615 K) shown in Figure 5a. Thus, it is clear that the E/T analysis provides a very accurate method of measuring the temperature of hot gases in flame reactors.

Soot formation

Soot is observed in the radiance (emission) measurements of the TTIP–CH_4 flames, and it presumably comes from the pyrolysis reactions of TTIP and CH_4. Prior to reaching the flame front, we expect the TTIP to pyrolyze at the C—O bonds, resulting in TiO_x species and C3 species. The C3 species can then form some soot early in the flame that then burns out downstream. Consistent with this interpretation is the fact that the TTIP flame is white-yellow in color, indicating some soot formation. The flame is more yellow in color at the lower center positions of the flame, and more white at the outer edges and higher positions in the flame.

Figure 6 shows the radiance spectra taken at 5 and 45 mm above the burner tip for flames containing different TTIP mass flow rates: (a) 4 g/h , (b) 11 g/h, and (c) 15 g/h. At the low TTIP flow rate [TTIP = 4 g/h (Figure 6a)], no significant concentration of soot is detected at either the 5- or the 45-mm positions. However, at higher TTIP flow rates, the spectra taken at 5 mm clearly show the presence of soot, as seen in the shift of the base-line radiance spectra above zero (Figures 6b and 6c). The radiance spectra at 45 mm are also shown to illustrate how the base-line radiance disappears when the soot has presumably been burned off.

For each radiance spectra of the flame (where this shift is present), a best fit is used to calculate temperature and concentration of the soot. The calculation assumes that the absorption coefficient of soot is proportional to $\upsilon^{0.83}$ (Köylu and Faeth, 1996). As a result, we can fit the base-line radiance to a function $R_{\text{soot}}(\upsilon) = \text{constant} \times \upsilon^{0.83} \times BB(\upsilon, T_s)$ in the wavenumber ranges of 2,630–5,900 and 6,100–6,500 cm^{-1}. The constant and T_s are treated as adjustable. The calculated soot fits are also included in Figure 6 for the radiance spectra at 5 mm. Table 2 shows the soot temperature for the different locations above the burner for TTIP mass flow rates of 11 and 15 g/h. The soot temperature seems to increase with increasing height (except at the highest position), but the soot temperature is always less than the gas temperature (Table 2). This observation is consistent with the previous results of Best et al. (1991), in which the local soot temperatures were up to 360 K lower than the local gas temperature. Our larger temperature differences may be due to the averaging along the line of sight and the fact that the soot may be located in a cooler part of the flame (on average) than the gas.

Once the temperature of soot is determined from the radiance spectra, we can then determine the relative amount of soot in the flame by calculating the amount of soot absorption from $[1-\tau(\upsilon)]_{\text{soot}} = R(\upsilon)/R_{\text{soot}}(\upsilon)$. The spectral region

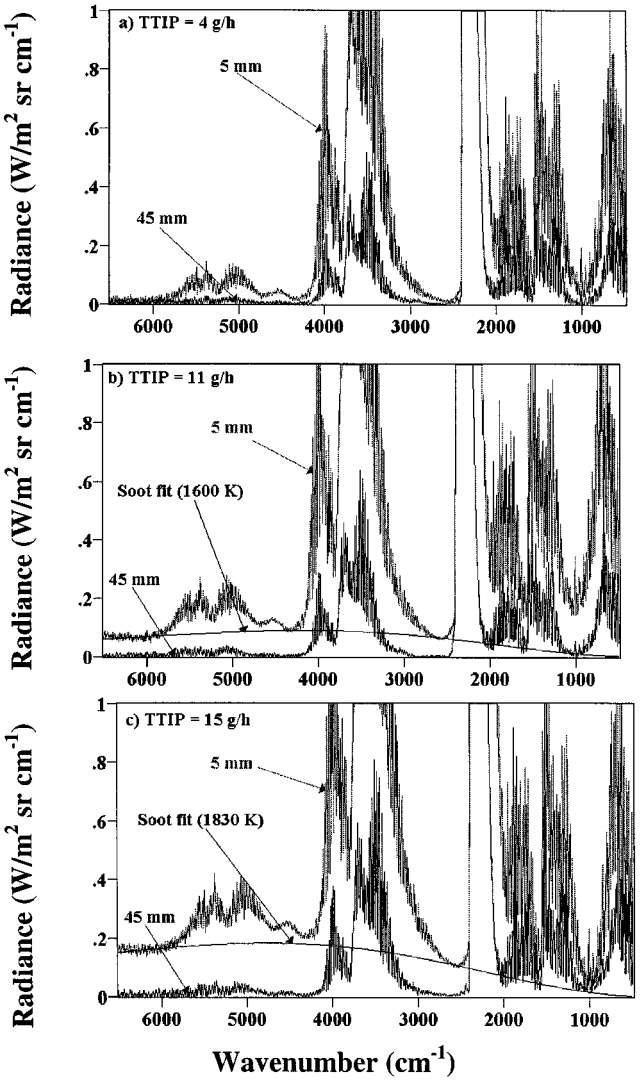

Figure 6. *In situ* radiance spectra of TTIP–CH_4 flames taken at 5 mm and 45 mm above the burner.

The TTIP flow rates are: (a) 4 g/h, (b) 11 g/h, and (c) 15 g/h. Soot temperature spectra fits are shown for the 5-mm position.

near 2,600-cm^{-1} is chosen since there are no species present in that region. The soot amount can then be put on an absolute basis by performing a carbon balance on the flame. The

Table 2. Soot Temperature for TTIP Mass Flow Rates vs. Average Flame Temperature Estimated by E/T analysis

Location Above Burner (mm)	TTIP = 11 g/h		TTIP = 15 g/h	
	Temp. of Soot (K)	E/T Temp. of Flame (K)	Temp. of Soot (K)	E/T Temp. of Flame (K)
3	1,353 ± 143*	2,083 ± 37	1,365 ± 84	2,129 ± 71
5	1,505 ± 96	2,155 ± 85	1,754 ± 6	2,193 ± 48
15	1,629 ± 4	2,018 ± 53	1,773 ± 26	2,088 ± 33
25	1,555 ± 42	1,705 ± 40	1,698 ± 36	1,946 ± 71
35	N/A	1,418 ± 22	1,629 ± 46	1,801 ± 94

*The ± values indicate the reproducibility of each measurement.

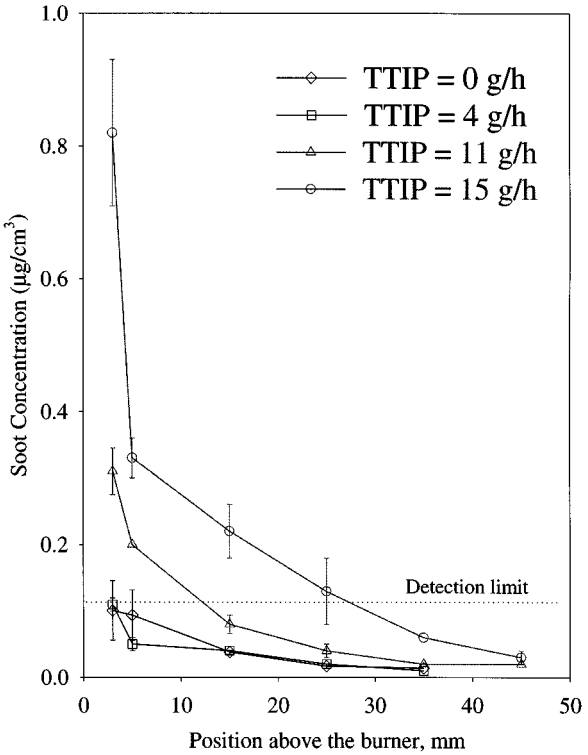

Figure 7. Soot concentration as a function of vertical position above the burner for the different TTIP mass flow rates.

The symbols correspond to an average of two experiments.

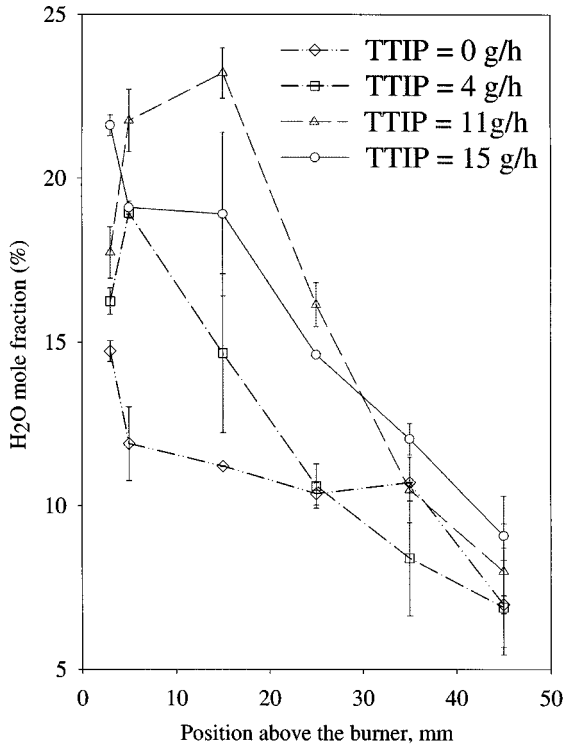

Figure 8. Mol fraction of H_2O for various TTIP–CH_4 flames at different vertical positions above the burner.

The mol fractions were determined using the average temperature determined by E/T analysis and calibration spectra calculated using the HITEMP database.

μg/cm^3 relative concentration of soot is calculated by comparing the CO_2 concentration in a TTIP–methane flame to the CO_2 concentration in the methane flame after taking the temperature into consideration (see calculations in Arabi-Katbi, 1999). We perform this calibration using a TTIP mass flow rate of 15 g/h and spectra taken at 3 mm above the burner. The flame diameter is 2 cm, the temperature is 2,200 K, and the total flow rate is 2,900 l/h. Under these conditions, calculations show that approximately 10% of the carbon in the reactants (TTIP and CH_4) does not completely burn to CO_2 (at 3 mm above the burner). Knowing the molar flow rate of carbon (mol/h) in the feed and assuming all the unburned carbon is soot, we thus estimate that the measured value of $[1-\tau(2{,}600\text{-cm}^{-1})]_{\text{soot}} = 0.0102$ corresponds to 0.71 μg of soot/cm^3.

Using the preceding calibration factor, Figure 7 shows the soot concentration (μg/cm^3) in the flame for the different TTIP mass flow rates. The soot concentration decreases with height due to soot oxidation in the flame. A soot concentration of 0.1 μg/cm^3 indicates negligible concentrations and that most of the carbon has burned to CO_2. In the case of 4 g/h, there are only negligible amounts of soot, which is similar to the TTIP-free methane flame. In the cases of the 11 g/h and 15 g/h flame, the soot completely burns off at 25 and 35 mm, respectively, above the burner. Note that the volumetric flow rates of methane and oxygen are kept the same at the different TTIP mass flow rates, so any additional carbon in the flame is a result of increasing the TTIP mass flow rate.

Axial distribution of H_2O

Figure 8 shows the mol fraction of H_2O for the different TTIP-methane flames as calculated using simulated spectra at the measured gas temperature. The error bar indicates the experimental range of each experimental condition; at least two experiments were taken for each point. In the methane flame (TTIP = 0 g/h), the mol fraction of H_2O decreases with position in the flame, which can be attributed to the dilution of the gases above the burner (Morrison et al., 1997). For the TTIP flames, however, the mol fraction of H_2O increases first between locations 3 and 15 mm above the burner before decreasing at higher positions due to dilution. At higher locations (higher than 25 mm), the mol fractions of H_2O in the TTIP flame are similar to the TTIP-free methane flame. Furthermore, although the measured H_2O fractions at $z = 3$ mm tend to agree well with a mass balance (except at the highest TTIP rate), the measured H_2O fractions in the TTIP flames at $z = 5$ tend to be higher than predicted from a mass balance. (The theoretical H_2O mol fractions are 14.5%, 16.6%, 17.2% and 18% for TTIP mass flow rates of 0, 4, 11, and 15 g/h, assuming complete combustion, no dilution, and taking into consideration the temperature and total flow rate.) At locations below 15 mm, the TTIP flames have measured H_2O fractions that can exceed the mass balance by 20–30%, particularly for the TTIP flow rate of 11 g/h.

Two possible explanations can account for these overestimates. One possibility is that the temperature is off by

20–30% (400–600 K), which primarily affects the concentration via the ideal gas law; the other possibility is that the local flame diameter is larger than the estimated diameter by 20–30% (2.4–2.6 cm rather than 2 cm). If either explanation were true, then the *calculated* absorbance is smaller than it should be, and we thus overestimate the measured concentration by about 20–30% to compensate for that error. Considering radial and axial temperature distributions and the uniformity of the burner, the possibility that the E/T temperature is off by 400–600 K is not likely; 100–200 K is more realistic. On the other hand, although we assume flame diameter is equal to the burner diameter, the local flame diameter may be bigger due to flickering, jet spreading and/or radial diffusion. Note that the TTIP flames have more flickering, have a higher temperature (which should cause more jet spreading), and higher gradients in water concentration. Thus, the second effect is a more realistic explanation for the discrepancies between the measurements and the mass balance.

TiO_2 spectral features

We have also attempted to isolate the absorption bands of the TiO_2 particles ($\sim$ 735-cm^{-1}) that lie beneath the hot H_2O and CO_2 features. The oxidation of both CH_4 and TTIP generates a large excess of H_2O and CO_2 for every mol of TiO_2. Removing these features cannot be done accurately enough unless we have very accurate H_2O and CO_2 spectra, either via simulation or experiment. Given that our temperature measurements are line of sight, we cannot currently calculate H_2O and CO_2 spectra accurately enough to reveal the small TiO_2 features except at positions where the gas is cool ($\sim$ 700 K). As an alternative, we have developed a different strategy of experimentally generating the required CO_2 and H_2O spectra by replacing the TTIP with acetone. The acetone produces no TiO_2 particles, provides additional hydrocarbon to generate H_2O and CO_2, and contributes fuel value to keep the temperature profile of the acetone flame roughly similar to the TTIP flame. Using spectra from the acetone–CH_4 flame, we can then subtract out the interfering H_2O and CO_2 bands to reveal the TiO_2 feature.

Figure 9a shows simulations of the absorption features of rutile TiO_2 particles for different particle shapes using Rayleigh extinction theory (Bohren and Huffman, 1983). We have simulated spectra for two cases, monodisperse spheres, and a continuous distribution of ellipsoids (CDE). These distributions approximate the two limiting forms that the particles may have in the flame: isolated TiO_2 spheres (spheres) or TiO_2 aggregates (CDE). These calculations are done using rutile TiO_2 optical constants at room temperature and assuming a concentration of 3 $\mu g/cm^2$ (which corresponds to a complete combustion of TTIP at a mass flow rate of 15 g/h). Figure 9a shows that the simulated TiO_2 bands appear around 735-cm^{-1}, and are very small in comparison to the measured bands of H_2O and CO_2.

For a low temperature spectrum, we have been able to isolate a portion of the predicted TiO_2 feature by subtracting the CO_2 and H_2O features using calculated spectra. At a downstream position of 120 mm, the E/T gas temperature is 700 K, and the large H_2O and CO_2 features are not nearly as widespread across the 900–500-cm^{-1} region because of the

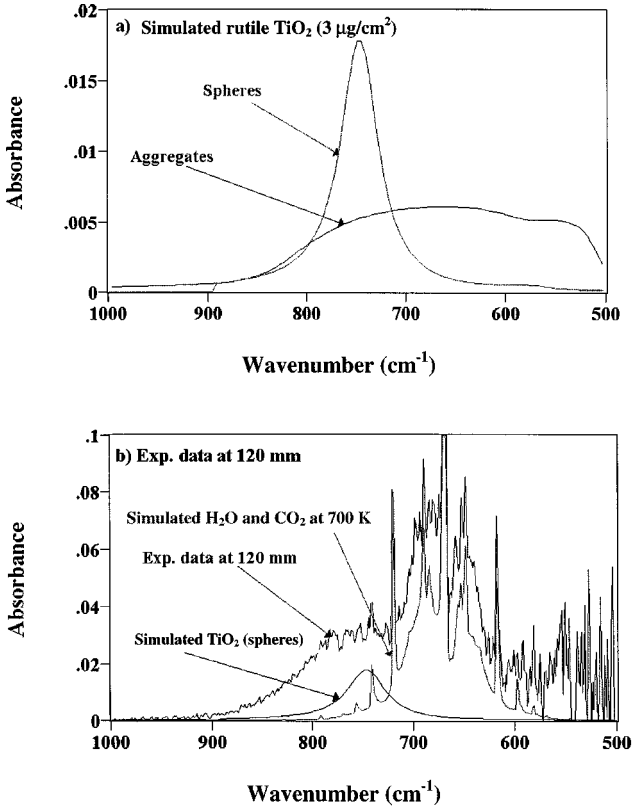

Figure 9. Absorbance spectra of TiO_2 bands (735 cm^{-1}).

(a) simulated spectra for rutile TiO_2 (3 $\mu g/cm^2$) spherical and aggregated particles; (b) experimental spectrum of a TTIP flame (15 g/h) at 120 mm above the burner. Also shown is a simulated spectrum for H_2O and CO_2 at the local temperature (700 K).

temperature narrowing of the rovibrational bands. Figure 9b shows the experimental absorbance of the gases at TTIP = 15 g/h; also shown are the simulated H_2O and CO_2 spectra at 700 K, scaled to match roughly the observed CO_2 and H_2O. Note that a shoulder appears near the CO_2 band at around 800–730-cm^{-1}, and we attribute this feature to the small amounts of TiO_2 in the flame. A methane (or acetone) flame does not show this shoulder.

The preceding strategy will not work at positions where the flame is hotter because the line-of-sight temperature is not sufficiently accurate to permit adequate simulation of the spectra. We can achieve the same result experimentally, however, if we use an acetone–CH_4 flame as a stand-in for the TTIP–CH_4 flame. Ideally, we would adjust the amount of acetone entering the CH_4 flame to match (1) the H_2O and CO_2 concentrations, and (2) the temperature distribution in the TTIP flame. Satisfying both of these conditions simultaneously is not possible because the stoichiometry and fuel value of the acetone does not match TTIP. On the other hand, matching the concentrations is not nearly as important as matching the temperature, since we can always mathematically scale the H_2O and CO_2 absorbance spectra to match the spectra in the TTIP flame. Consequently, our first priority has been to generate hot H_2O and CO_2 spectra by adjusting the acetone flow rate until it produces a flame with a

similar E/T temperature as the TTIP flame.

Such IR measurements of acetone and TTIP flames have been taken at 5 mm above the burner, and the TTIP flame is run at 15 g of TTIP/h. Visually, the acetone–methane flame is cone-shaped and is similar to the TTIP–methane flame. Both of these flames are different from the methane flame, which looks like a flat flame less than 5 mm high. However, the TTIP–methane flame is white-yellow in color compared to the blue of the acetone–methane or methane flames. On a coarse scale, the temperature-matching procedure has produced qualitatively similar absorbance spectra. The only significant distinction is that the acetone flame has a CO band (2,050-cm^{-1}) that is not observed in the other flames. This is the result of the flame being fuel-rich, thus causing incomplete combustion. Although soot and CO are also observed at 5 mm above the burner in the acetone–methane flame, they are no longer observed at 25 mm above the burner, presumably due to the complete oxidation of the species.

We can further improve the matching of the acetone flame to the TTIP flame by scaling the H_2O spectrum in the acetone flame to match the TTIP flame. We use the least-square fit discussed earlier and perform the match in the wavenumber 1,600–1,000-cm^{-1} range. We use this region because it has no TiO_2 features. Then, we subtract the scaled acetone–CH_4 flame spectrum from the TTIP–methane flame spectrum to remove the H_2O features in 1,000–500-cm^{-1} region. Although this procedure works extremely well on the H_2O features, it tends to remove slightly too much of the CO_2 features in the 1,000–500-cm^{-1} region, because the H_2O/CO_2 stoichiometry is different in the acetone–CH_4 flames and the TTIP–CH_4 flames. Overremoving the CO_2 features is not an issue, however, since the CO_2 spectrum is rather distinctive compared to the two possible spectra of the TiO_2 particles (Figure 9b).

Figure 10 shows the result of subtracting the reference acetone–CH_4 spectrum from the TTIP–CH_4 flame spectrum at locations 5, 15, and 45 mm above the burner (TTIP = 15 g/h). The figure shows the resultant spectra to have a residual feature that roughly corresponds to the prediction of the simulated TiO_2 spectra. The residual spectra do not seem to change with axial position, and the feature shape matches the shape of the CDE distribution, but not its magnitude. To understand this discrepancy better, we have examined transmission electron microscope (TEM) pictures of the particles collected by thermophoretic sampling at the same locations (Arabi-Katbi, 1999). The TEM images [see Arabi-Katbi et al. (2000)] show that the particles are somewhat aggregated at the 5-mm location, but more spherical at 45 mm. Thus, the TEM indicates that the FTIR spectra should exhibit CDE spectral features close to the burner and more "spherical" spectral features at high axial positions (Figure 9a).

Experimentally, the FTIR spectra do not exhibit such changes. Part of the problem may be that there is a large amount of noise in the spectra as well as a very small amount of TiO_2, which makes it more difficult to detect any changes, as predicted by Figure 9a. In addition, approximating the extinction of the aggregates using the CDE may not be valid. Figures 9b and 10 also show that the TiO_2 band may be shifted toward higher wavenumbers than predicted by Figure 9a. This shift may be due to the temperature dependence of the optical constants of TiO_2 or because we use the optical constants for rutile instead of anatase (Morrison et al., 1997).

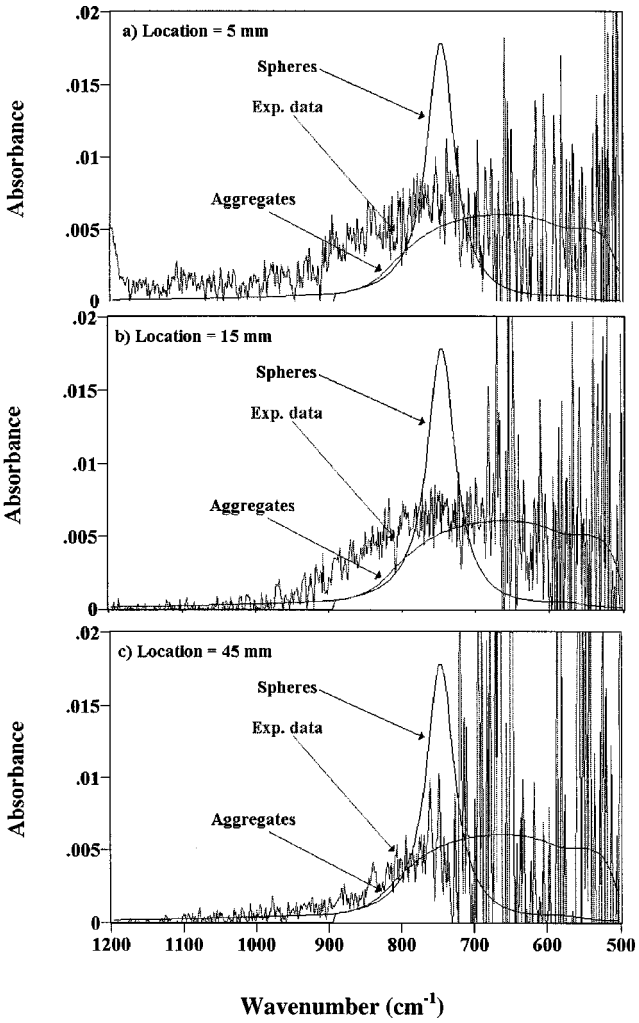

Figure 10. *In situ* absorbance spectra of TiO_2 bands (735-cm^{-1}) calculated by subtracting the adjusted absorbance of an acetone flame from the absorbance of the TTIP flame (15 g/h): (a) 5 mm, (b) 15 mm, and (c) 45 mm above the burner tip.

The X-ray diffraction results on the particles show them to be mostly anatase (Arabi-Katbi, 1999), but the optical constants for anatase are not available. For 45 mm above the burner, the TiO_2 bands seem to be a better fit (in the 1,000–750-cm^{-1} region) with the simulated band, perhaps due to the lower temperature at this location (1,550 K).

Conclusions

FTIR emission/transmission (E/T) analysis is performed on hot gases of a premixed methane flame. The flame temperature determined by E/T is found to be in very good agreement with the temperature measurements from a thermocouple. The graybody best fit shows excellent agreement with the readout temperature of the surface of the thermocouple. Using a standard correction to convert the thermocouple temperature to a gas temperature, we find that the

E/T temperature and the thermocouple gas temperature agree quite well when an emissivity of 0.57 is used. In correcting for heat radiation loss from thermocouples, estimating the emissivity factor is very important in obtaining accurate corrections.

FTIR data indicate the presence of soot in the titanium tetraisopropoxide–CH_4 (TTIP–CH_4) flame. The soot concentrations decrease to negligible concentrations at 35 mm above the burner at the highest TTIP flow rates, due to oxidation higher in the flame. The soot temperature is always lower than the average flame temperature, as observed previously in ethylene diffusion flames (Best et al., 1991).

The HITRAN and HITEMP databases are used to calculate the mol fraction of H_2O and CO_2 in the flame at different positions. In general, the TiO_2 particle features are not directly observable without subtracting out the interfering H_2O and CO_2 features from the spectra. However, the noise in the FTIR spectra as well as the small absorbance bands of TiO_2 makes it difficult to extract the TiO_2 features unless the gas temperature is low ($\sim$ 700 K). An alternative method of extracting the TiO_2 features is possible by experimentally generating flame spectra without TiO_2 and subtracting them from the TTIP–CH_4 flame spectra. We have used acetone–CH_4 flames to generate the necessary spectra. After adjusting the acetone flow rate to match the temperature found in the TTIP–CH_4 flame, we rescale the synthetic spectrum to eliminate the H_2O and CO_2 interferences and reveal the TiO_2 features. These features are broad and roughly match the predictions of Rayleigh extinction theory.

The findings in this article also point to the need for tomography to improve measurements of the concentration and temperature profiles of the flame. Such point information will help improve the interpretation of the FTIR spectra.

Acknowledgments

The support by the U.S. National Science Foundation through Grants CTS-9619392 (SEP) and CTS-9625095 (PWM) are greatly appreciated.

Literature Cited

Arabi-Katbi, O. I., S. E. Pratsinis, P. W. Morrison, Jr., and C. M. Megaridis, "Monitoring of Flame Synthesis of Titania Nanoparticles by *In Situ* Fourier Transform Infrared (FTIR) Spectroscopy and Thermophoretic Sampling," *Combust. Flame*, **124**, 560 (2000).

Arabi-Katbi, O. I., "Flame Synthesis of Titania Nanoparticles: Analysis Using In Situ Fourier Transform Infrared (FTIR) Spectroscopy and Thermophoretic Sampling," MS Thesis, Univ. of Cincinnati, Cincinnati, OH (1999).

Bengtsoon, P. E., L. Martinsoon, M. Alden, and S. Kröll, "Rotational CARS Thermometry in Sooty Flames," *Comb. Sci. Technol.*, **81**, 129 (1992).

Best, P. E., R. M. Carangelo, J. R. Markham, and P. R. Solomon, "Extension of Emission-Transmission Technique to Particulate Samples Using FT-IR," *Combust. Flame*, **66**, 47 (1986).

Best, P. E., P. L. Chien, R. M. Carangelo, P. R. Solomon, M. Danchak, and I. Ilovici, "Tomographic Reconstruction of FT-IR Emission and Transmission Spectra in a Sooty Laminar Diffusion Flame: Species Concentration and Temperatures," *Combust. Flame*, **85**, 309 (1991).

Boedeker, L. R., and G. M. Dobbs, "Soot Distribution and CARS Temperature Measurements in Axisymmetric Laminar Diffusion Flames with Several Fuels," *Proc. Int. Symp. on Combustion*, The Combustion Institute, Baltimore, p. 1097 (1986).

Bohren, C. F., and D. R. Huffman, *Absorption and Scattering of Light by Small Particles*, Wiley, New York (1983).

Collis, D. C., and M. J. Williams, "Two-Dimensional Convection from Heated Wires at Low Reynolds Numbers," *J. Fluid Mech.*, **6**, 357 (1959).

Farrow, R. L., R. P. Lucht, W. L. Flower, and R. E. Palmer, "Coherent Anti-Stokes Raman Spectroscopic Measurements of Temperature and Acetylene Spectra in a Sooting Diffusion Flame," *Proc. Int. Symp. on Combustion*, The Combustion Institute, Baltimore, p. 1307 (1984).

Govatzidakis, G. J., "Thermocouple Thermometry in Soot Bearing Flames," BS Thesis, Brown University, Providence, RI (1993).

Griffiths, G. J., and J. A. de Haseth, *Fourier Transform Infrared Spectrometry*, Wiley, New York (1986).

Kent, J. H., and H. G. Wagner, "Why Do Diffusion Flames Emit Smoke?" *Comb. Sci. Technol.*, **41**, 245 (1984).

Köylu, Ü. Ö., and G. M. Faeth, "Spectral Extinction Coefficients of Soot Aggregates from Turbulent Diffusion Flames," *J. Heat Transfer*, **118**, 415 (1996).

Lide, D. R., *CRC Handbook of Chemistry and Physics*, 72nd ed., CRC Press, Boston, MA (1982).

Madson, J. M., and E. A. Theby, "SiO_2 Coated Thermocouples," *Comb. Sci. Technol.*, **36**, 205 (1984).

Markham, J. M., Y. P. Zhang, R. M. Carangelo, and P. R. Solomon, "FT-IR Emission/Transmission Tomography of a Coal Flame," *Proc. Int. Symp. on Combustion*, The Combustion Institute, Baltimore, p. 1869 (1990).

Morrison, P. W., Jr., and J. R. Haigis, "In Situ Infrared Measurements of Film and Gas Properties During the Plasma Deposition of Amorphous Hydrogenated Silicon," *J. Vac. Sci. Technol. A*, **11**, 490 (1993).

Morrison, P. W., Jr., R. Raghavan, A. J. Timpone, C. P. Artelt, and S. E. Pratsinis, "*In Situ* Fourier Transform Infrared Characterization of the Effect of Electrical Fields on the Flame Synthesis of TiO_2 Particles," *Chem. Mater.*, **9**, 2702 (1997).

Morrison, P. W., Jr., J. E. Cosgrove, J. R. Markham, and P. R. Solomon, "In Situ IR Spectroscopy of an Oxygen-Acetylene Flame During Diamond Film Growth," *Carbon*, **28**, 767 (1990).

Morrison, P. W., Jr., and O. Taweechokesupsin, "Calculation of Gas Spectra for Quantitative Fourier Transform Infrared Spectroscopy of Chemical Vapor Deposition," *J. Electrochem. Soc.*, **145**, (9), 3212 (1998).

Solomon, P. R., P. E. Best, R. M. Carangelo, J. R. Markham, P-L. Chien, R. J. Santoro, and H. G. Semerjian, "FT-IR Emission/Transmission Spectroscopy for In Situ Combustion Diagnostics," *Proc. Int. Symp. on Combustion*, The Combustion Institute, Baltimore, p. 1763 (1986).

Solomon, P. R., and P. E. Best, "Fourier Transform Infrared Emission/Transmission Spectroscopy in Flames," *Combustion Measurements*, N. Chigier, ed., Hemisphere Publishing Corp., New York, pp. 385–444 (1991).

Rothman, L. S., R. Gamache, A. Goldman, L. Brown, R. Toth, H. Pickett, R. Poynter, J. Flaud, C. Camy-Peyret, A. Barbe, N. Husson, C. Rinsland, and M. Smith, "The HITRAN Database: 1986 Edition," *Appl. Opt.*, **26**, 4058 (1987).

Rothman, L., R. Gamache, R. Tipping, C. Rinsland, M. Smith, D. Benner, V. Malathy Devi, J. M. Flaud, C. Camy-Peyret, A. Perrin, A. Goldman, S. Massie, L. Brown, and R. Toth, "The HITRAN Molecular Database: Edition of 1991 and 1992," *J. Quant. Spectrosc. Radiat. Transfer*, **48**, 469 (1992).

Vemury, S., and S. E. Pratsinis, "Charging and Coagulation During Flame Synthesis of Silica," *J. Aerosol Sci.*, **27**, 951 (1996).

Vijayakumar, R., and K. T. Whitby, "Flat Flame Ultrafine Aerosol Generator," *Aerosol Sci. Technol.*, **3**, 17 (1984).

Manuscript received Feb. 6, 2001, and revision received July 9, 2001.